

Core Sample Permeability Estimation Using Statistical Image Analysis

Ioannis Chatzis*, Derrick M. Jewlal and Marios A. Ioannidis

Department of Chemical Engineering

Porous Media Research Institute

University of Waterloo, Waterloo, Ontario, Canada, N2L 3G1

ABSTRACT

The statistical description of pore space seen in a 2-D section has been successfully applied for the characterization of the pore structure of different types of porous media using 1) the optical porosity and 2) the spatial distribution of porosity, which can be described by the autocorrelation function (ACF) of pore space seen in 2-D space. Statistics obtained from images include the image porosity, specific surface area, and a length scale obtained from the integral of the image autocorrelation function. The number of images required to predict the permeability of a core sample accurately, using the porosity (ϕ_i) and the integral scale of the autocorrelation function for an image (I_i), is addressed in this paper. The following phenomenological permeability model was found to describe the behavior of many samples:

$$k = A \langle \phi_i \rangle^B \langle I_i \rangle^C$$

where k is the predicted absolute permeability of the sample, $\langle \phi_i \rangle$ and $\langle I_i \rangle$ are the average porosity and average integral scale of ACF of all images respectively, while A , B , and C are parameter values determined by fitting experimentally determined permeabilities of tested core samples. The proposed correlation accounts not only for reservoir porosity, but also the pore structure characteristics of the medium as determined from statistics of 2-D images. The proposed form of permeability correlation is more robust than other similar methods. Furthermore, at least 10 randomly taken images from a section are required to make a reasonable estimate of the permeability of a core sample. The permeability distribution at the scale of 512 by 512 pixels with 1.5 microns resolution can be estimated using Monte Carlo trials if the number of images taken for any given sample is 40 or greater.

INTRODUCTION

It is possible to obtain valuable information for property estimation by analyzing images of reservoir core samples. If the pore structure of a sample is "random", then the porosity of the specimen is equal to the "optical porosity", which can be determined from polished thin sections (Dullien, 1992). Normally, it is necessary to impregnate the pores with a substance such as epoxy resin or Wood's metal (a low melting point alloy) in order to make the pores more visible. Experimental data regarding pore throats and pore bodies have been acquired by the image analysis of pore casts using serial sectioning techniques (Dullien and Dhawan, 1974; Wardlaw and Cassan, 1978; Koplik *et al.*, 1984; Kwiecien *et al.*, 1990; Lymberopoulos and Payatakes, 1992). The analysis of capillary and transport phenomena in porous media using network models of pore structure by various authors (e.g., Dullien, 1992; Ioannidis and

Chatzis, 1993; Bryant *et al.*, 1993) have demonstrated the importance of the size distribution of pore throats and pore bodies, the connectivity of the porous network and the spatial correlation of pore sizes. Unfortunately, none of these important aspects can be reliably estimated from 2-D images because the actual 3-D pore structure appears as a set of disconnected void regions which cannot be definitively linked to particular features which we refer to as pores bodies, or pore throats.

In an attempt to overcome these limitations (Ehrlich *et al.*, 1991; Ferm *et al.*, 1993; Bowers *et al.*, 1994), empirical models have been proposed which couple data obtained from both mercury porosimetry experiments and 2-D image analysis for permeability predictions. Recognizing that explicit pore throat information is absent from 2-D images and that mercury porosimetry data only provide information regarding pore volumes accessed by throats of a certain size, these correlations were applied to selected data sets with some success (Coskun and Wardlaw, 1993), it has yet to be demonstrated that they can be generally applicable for different types of porous media.

Despite recognized limitations of pore structure information conveyed by 2-D image data, significant correlations have been identified between permeability and 2-D geometrical features of pore structure data (Berryman and Blair (1986 & 1987), Coskun and Wardlaw, 1993). Coskun and Wardlaw (1993) developed an empirical model which can explain the variance in permeability of over 50 sandstone samples using a diameter distribution of the largest inscribed circles ("pore" diameters) within visible 2-D void spaces on petrographic thin sections. Their success is attributable to the correlation between the 2-D pore sizes and the pore throat sizes which control permeability in 3-D networks. Although such correlations are likely not universal for widely different materials, the work of Coskun and Wardlaw (1993) does nevertheless corroborate similar observations made by other investigators (Yuan, 1989; Ehrlich *et al.*, 1991; McCreech *et al.*, 1991).

Berryman and Blair (1986 & 1987) proposed a correlation for permeability which follows the form of the well known Kozeny-Carman relation, as shown below:

$$k_{KC} = \phi^2 / bFS^2 \quad (1)$$

where ϕ is the porosity, b is a shape factor ($2 < b < 3$), F is the formation resistivity factor, and S is the specific surface area. Although this simple correlation performs surprisingly well (Jewlal, 1996), the authors faced a problem in extracting the required image statistics (e.g., porosity and specific surface area). They contended that for accurate porosity estimates one image magnification is required, however, another magnification of the image is required to produce the necessary specific surface area needed in Eq.(1) to make accurate prediction of permeability. The "optimum" image magnification factor is not known a priori, and the uncertainty in estimating F and S from image analysis is a major weakness of this approach.

Because of the inherent difficulties in estimating accurately the specific surface area from image analysis, the work of Ioannidis *et al.* (1995, 1996) demonstrated that the average of the integral scale of the ACF's of pore space seen in 2-D images of a polished section along with the average porosity of a core sample are sufficient parameters to predict the permeability using a phenomenological model. This problem was addressed in detail by Jewlal (1996) and the intent of this paper is to present the key findings for permeability estimation using statistical parameters obtained from 2-D image analysis.

THEORY

It is generally accepted that bulk porosity has a strong influence on the permeability of a porous medium. However, the manner in which the porosity is distributed is of critical importance and can be quantified only by way of a statistical analysis at the sub-pore scale. So far, the parameter which has been expected to reflect to some degree the spatial variation of porosity is the formation factor, F . Several correlations between permeability, porosity and formation factor have been proposed (Katz and Thompson, 1986; Dullien, 1992), but no unique correlation will accurately predict permeability for all media.

An n -point correlation function in image analysis measures the probability that n points in a specified geometrical arrangement all reside in the phase of interest within a two phase system (defined by the phase function). For example, the one-point correlation function is the probability that any point lies in the phase of interest. If the phase function is defined for every possible point within the system, then the mean of the one-point correlation function over the space will produce ϕ , the porosity:

$$\hat{S}_1 = \langle f(x) \rangle = \phi \quad (2)$$

The brackets $\langle \rangle$ indicate a volume average over the spatial coordinate x .

The two point correlation, is the probability that two points a specified distance apart are both within the phase of interest. As described in detail by Berryman and Blair (1985), it provides a great deal more information and is defined as follows:

$$\hat{S}_2(r_1, r_2) = \langle f(x+r_1)f(x+r_2) \rangle \quad (3)$$

where r_1 and r_2 are distances (lags) from the reference point x . If homogeneity and isotropy can be assumed, then the two-point correlation function can be simplified to:

$$\hat{S}_2(r_1, r_2) = S_2(|r_2 - r_1|) \quad (4)$$

The three-point correlation function is the probability that all three vertices of a specified triangle lie in phase one. It is defined as follows:

$$\hat{S}_3(r_1, r_2, r_3) = \langle f(x+r_1)f(x+r_2)f(x+r_3) \rangle \quad (5)$$

Since two points can be found on a line, and three points lie on a surface, it is possible to measure \hat{S}_1 , \hat{S}_2 , and \hat{S}_3 by analyzing data in 2-D images. Only the one-point and the two-point correlation function statistics were used in our work.

Investigations involving correlation function statistics in image analysis were first attempted by Corson (1974), who took photographs of selected material, magnified, and then aligned a grid upon them. This formed the basis for recording the values designating either rock or pore space at each grid point manually. The correlation functions were then calculated from the tabulated data. This method however was tedious, since it required an operator to view each point and to assign each individual grid location a value. An elegant method to obtain the same information using modern image processing techniques was pioneered by Berryman (1985, 1987). The autocorrelation function $R_z(\vec{r})$ is a normalized form of the two-point correlation function $S_2(\vec{r})$, employed by others (Berryman and Milton, 1985; Berryman and Blair, 1986 & 1987), and is calculated by the relation:

$$R_z(\bar{r}) = \frac{S_2(\bar{r}) - \phi^2}{\phi - \phi^2} \quad (6)$$

For images of many samples, Ioannidis *et al.* (1996) found the following analytical model to fit the average autocorrelation function data very well:

$$R_z(\bar{r}) = \exp\left[-\left(\frac{r}{\lambda}\right)^n\right] \quad (7)$$

where the shape parameter n and the correlation length λ of the ACF are obtained by fitting the average ACF data of a sample. The autocorrelation function, $R_z(\bar{r})$, is a measure of the probability that given a void pixel within the medium, another void pixel is located a distance \bar{r} away. Naturally, porous media composed of larger pore spaces will have autocorrelation functions which look significantly different than those produced from rocks with scattered porosity configured in smaller pore spaces. In an attempt to quantify this difference, the integral of the autocorrelation function can be employed as the discriminating statistic property (Ioannidis *et al.*, 1996).

The integral scale of an ACF, $I = \int_0^{\infty} R_z(\bar{r}) d\bar{r}$, can be determined by numerical integration of Eq(6), or analytically, by taking the integral of Eq.(7). The magnitude of this integral is directly proportional to the average size of the sections of pore space seen on 2-D images. Since media composed of smaller pores will produce autocorrelation functions that will drop off quickly to zero at shorter lags, the resulting integral will be likewise quite small. When the pore spaces are large, the autocorrelation function will remain at a significant value for larger lags and will produce a larger integral. Thus, the value of the resulting integral can be viewed as an indication of the characteristic size of the pore spaces visible in a 2-D section of a porous material. With the set of average porosity and integral scale values, we can differentiate porous media by way of their autocorrelation function. Figures 1 and 2 show typical behaviour of the ACF and the 2-point correlation function of a sample.

Another important property of the two-point correlation function (for isotropic porous media) is the slope of the curve at the origin, which is used to estimate the specific surface area of the sample. Debye *et al.* (1957) derived the following result :

$$\lim_{r \rightarrow 0^+} \frac{dS_2(r)}{dr} = -\frac{A_s}{4V} \quad (8)$$

The derivative of $S_2(r)$ at the origin is related to specific surface area : $S_2'(0) = -S/4$ (9)

The specific surface area is defined as $S = A_s/V$, where A_s is the total surface area, and V the total volume. An estimate for the value of S is required when applying Eq.(1)

In our efforts in developing a computer enhanced core analysis (CECA) methodology for the prediction of numerous properties in our laboratory, it was found that the integral scale of the ACF of an image, I_i and the corresponding porosity of a 2-D image are independent variables (Jewlall, 1996; Ioannidis *et al.*, 1995, 1996). The following phenomenological model is proposed for permeability prediction only:

$$k = A \langle \phi_i \rangle^B \langle I_i \rangle^C \quad (10)$$

When multiple estimates for permeability are made on the same sample using different images from a section of a core sample, it is improper to attempt to pool the results using an arithmetic average. This would be akin to assigning the properties of an arbitrary region to the whole system, while discounting contributions from less representative portions, no matter how important they may be. Gelhar and Axness (1983) have studied the problem of averaging the permeability of porous media composed of regions of different permeability which are correlated in space. Their work has shown that the best estimate for the effective permeability is computed by:

$$k_{eff} = e^{k_m} \left(1 + \frac{\sigma_k^2}{6} \right) \quad (11)$$

where k_m is the geometric mean of the permeability estimates, and σ_k^2 is the variance of the natural log of the permeability estimates. However, the arithmetic average is useful in the sense that it allows for a quantitative estimate of the variance of permeability estimates. Similar analysis is not possible with k_{eff} , as only a single value is produced.

Experimental Data

A large number of high quality back-scatter mode scanning electron images(BSE) for 14 core samples from 4 formations in Western Canada were used to investigate the relationship of sample permeability to core porosity and the integral of the ACF function, as part of the Computer Enhanced Core Analysis(CECA) project in our laboratory(Ioannidis et. al., 1995, 1996). BSE image data were obtained from a section of a core plug, measuring 3.8 cm in diameter, while the core permeability and porosity were measured in the rest of the core sample. About 60 BSE images per core sample, each consisting of 765 x 573 picture elements(pixels) were taken for statistical image analysis. The conventional core analysis property values and the statistical properties obtained by image analysis are summarized in Table 1. As seen in this table, permeability varied by three orders of magnitude. Additional images and core analysis data for sandstones investigated by Wardlaw and Coskun(1993) were also used by Jewlral(1996) and Ioannidis et. al. (1996) for comparison of the various models that use image analysis data to predict core permeability.

Results and Discussion

Integral vs Porosity Plots: A graphical representation of the relationship between image ACF integral, I_i , and image porosity, ϕ_i , was prepared for each of the CECA samples, showing the 95% joint confidence region for I_i and ϕ_i , as illustrated in Fig. 3 for sample 7. Typically, points which lie outside the ellipse correspond to statistical outliers at the designated confidence level. Up to about 20% of image data were found to fall outside the 95% confidence region(Jewlral, 1996). From the appearance of the results in Fig. 3, the parameters I_i and ϕ_i are independent. This behavior was found to apply for the rest of the CECA samples. The apparent independence of the two parameters, justifies the use of the empirical permeability model defined by Eq.(10). The composite scatter-plot, showing all 916 points which make up the CECA data set of the autocorrelation function integral scale I vs. ϕ plot is shown in Figure 4. It is clear that for the wide range of image porosity values which comprise the CECA data set, the corresponding ACF integral values exhibit no discernible trend with porosity values.

Figure 4 also illustrates that sample images of the Montney formation (a dolomite siltstone) are very different than the other formations due to the fine pore sizes present in them.

Parameter Estimates for the Empirical Permeability Model: Based on various methods described in Jewlal(1996), parameters for the model defined by Eq.(10), for various sets of image data. The empirical parameters A, B, and C were determined by fitting the data in a variety of ways mentioned in Table 2. For each of the methods used, a summary of the parameter values found is shown in Table 2. Utilizing these parameter values and information in Table 1, the predicted permeability values are shown in Table 3.

Upon examination of the squared sum of residual errors shown in Table 2, it is clear that employing all available CECA images data, produces a correlation with a poor ability to match the averaged CECA image data. The sum of residual errors squared in method (iii) seen in Table 2, is approximately twice that of the other methods, while the regression R^2 for the data is twenty per cent poorer. Clearly, without some averaging or filtering of the individual image data, outliers have a marked negative effect on the effectiveness of the model. Least squares regression R^2 and sum of residuals squared values are almost identical to those obtained by employing a simple averaging technique. This result indicates that the image data are indeed normally distributed, with outliers on the high and low ends. If the outlier data are removed, the 95% confidence region data set produces a similar result as the intact data set (see Table 3).

Comparison with other methods: Using the empirical model-iv parameter values (given in Table 2) in Eq.(10), the prediction of permeability from every image of the CECA data in the 95% joint confidence region of the I vs ϕ was made and the results are shown in Fig. 5(a). Similarly, using the estimated specific surface area of every image based on the two point correlation function of every image (e.g., using Eq.(8)) and the estimated formation resistivity factor F , based on image porosity (e.g., $F = \phi^2$), the permeability value by applying Berryman's approach via Eq.(1) was also calculated for every image. The calculated results are shown in Fig. 5(b), by plotting the image predicted permeability vs. the core measured permeability. Both approaches produce a spectrum of predicted permeabilities, however, the average value of permeability predictions by our method using model-iv parameter values are in better agreement with experimental values compared to the case of using Eq.(1). The drawback in applying Eq.(1) is the inherent uncertainty in the estimation of the specific surface area, which appears to be under-predicted. Jewlal(1996) showed that by increasing the magnification factor by a factor of two, the estimated surface area from the two-point correlation factor increased by 20%. Generally, for samples of low permeability, use of Eq.(1) with image derived parameter values for S tends to over-estimate the permeability value.

The images of sandstone samples obtained in the work of Coskun and Wardlaw (1993) were re-analyzed by Jewlal (1996) using the approach developed in the CECA project. Because of the low magnification factor used in acquiring these images, the reported core porosity value was used in applying the correlation of Eq.(10), because the average of image porosity values for any given sample were generally much lower than the measured core porosity. The integral scale of the ACF is not very sensitive to the magnification factor, as the relatively large pore features seen in 2-D images contribute the most for its value. Using the estimated parameter values of Eq.(10) by the image data base of CECA samples reported in Table 2 for model-iv, the predicted permeabilities for the samples tested by Coskun and Wardlaw (1993) have as shown

in Fig. 6. It is encouraging to see the parameter values obtained with the CECA data set were accurate enough to make excellent predictions of permeability values of other samples.

Effect of Number of Images: Available images from any core sample ranged from 41 to 75 images. Performing statistical significant tests on average image porosity versus core porosity (the only measured statistic with an available experimental value), it was found that groups of less than sixty randomly chosen images perform just as well as those with greater than sixty images. To explore the effects of the number of images used on the estimated permeabilities, Monte Carlo simulations were performed on each core sample to determine the variability in permeability predictions. The Monte Carlo simulation method involved the generation of random data sets with the same statistical properties as that of a known experimental sample. A computer program was coded which evaluated a large number of possible predictions of permeability based upon sets of 5, 10, 20, 40, and 60 images. The permeability predicted from an image was calculated using Eq.(10) and model-iv parameter values. In each realization with a set of 5, 10, , the arithmetic average, the geometric average, and the effective permeability computed by way of Eq.(11) were calculated respectively. By performing many trials, frequency distributions for the arithmetic mean, geometric mean, and effective permeability were obtained. Typical behavior for the CECA sample 7 is shown by the plots in Fig. 7. More details are provided elsewhere (Jewlral, 1996).

Based on Monte Carlo simulations, the mean of the predicted permeability using the arithmetic average is not sensitive to the number of images in a set. This distribution over-predicts the sample permeability estimated using the arithmetic average of all image porosities and the arithmetic average of all image integral scale, $\langle I \rangle$, shown to correspond to the dashed vertical line in Fig. 7. The mean of the predicted permeability distribution using the geometric average of a set decreases significantly as the number of images increases, and is the smallest of them. The mean of the K_{eff} permeability distribution decreases a little as the size of the set of images increases and is more close to experimental values. For sample 7, the mean of the K_{eff} distribution decreased as follows: 119 mD for 10 images, 114 mD for 20 images, and 112 mD for the case of sets with 60 images. All three distributions become narrower as the size of the set of images increases.

Conclusions

- The porosity and integral scale of the autocorrelation function were used to develop a correlation to predict formation permeability for the 14 samples of the CECA data set. The resulting correlations were able to predict accurately the permeability of samples.
- It was verified that the correlating parameters, namely, image porosity and image autocorrelation function integral, are sufficiently independent to warrant their use in a permeability model. It was also shown that simple averaging of image data is adequate to produce representative statistics for use in permeability correlations.
- It was found that individual images could easily provide unrepresentative sample data due to the variability encountered in the sample image data. However, when sufficient number of image data were available, image porosity accurately estimated that of the core.
- Monte Carlo simulations revealed that the number of images required for accurate prediction of permeability depends largely upon the variability of the sample being imaged. It was shown that there exists little incremental value in acquiring large data sets

in excess of approximately forty images. Furthermore, it was shown that the effective permeability model is an excellent predictor of formation permeability.

Acknowledgments

Funding for this research provided by NSERC, and the consortium companies supporting the CECA project (Canadian Hunter Exploration, Chevron Canada Resources, Gulf Canada Resources, Hycal Energy Laboratories, Husky Oil Exploration, Noranda, PanCanadian Petroleum and Suncor Resources), is gratefully acknowledged. The authors are indebted to Mr. Jon McGovern for obtaining the BSE images and to Dr. Norman Wardlaw for making available additional image analysis data for sandstone samples.

References

- Berryman, J. G. (1985). "Measurement of spatial correlation functions using image processing techniques." *Journal of Applied Physics*, **57**, (7), 2374.
- Berryman, J. G. (1987). "Interpolating and Integrating Three-Point Correlation Functions on a Lattice." *Journal of Computational Physics*, **75**, 86.
- Berryman, J. G., and Blair, S. C. (1986) "Use of digital image analysis to estimate fluid permeability of porous materials: Application of two-point correlation functions." *Journal of Applied Physics*, **60**, (6), 1930.
- Berryman, J. G., and Blair, S. C. (1987) "Kozeny-Carman relations and image processing methods for estimating Darcy's constant." *Journal of Applied Physics*, **62**, (6), 2221.
- Berryman, J. G., and Milton, G. W. (1985). "Normalization constraint for variational bounds on fluid permeability." *Journal of Chemical Physics*, **83**, (2), 754.
- Bowers, M. C., Ehrlich, R., and Clark, R. A. (1994). "Determination of petrographic factors controlling permeability using petrographic image analysis and core data, Satun Field, Pattani Basin, Gulf of Thailand." *Marine and Petroleum Geology*, **11**, (2), 148.
- Brace, W. F., Walsh, J. B., and Frangos, W. T. (1968). *Journal of Geophysical Research*. **73**, 2225.
- Bryant, S., Cade, C., and Mellor, D. (1993) "Permeability prediction from geologic models." *AAPG Bulletin*, **8**, 1338.
- Corson, P. B. (1974). *Journal of Applied Physics*, **45**, 3159.
- Coskun, S. B., and Wardlaw, N. C. (1993) "Estimation of permeability from image analysis of reservoir sandstones." *Journal of Petroleum Science and Engineering*, **10**, 1.
- Debye, P., Anderson Jr. H. R., Brumberger, H. (1957) *Journal of Applied Physics*, **28**, 679
- Dullien, F. A. L. (1992). "Porous Media, fluid transport and pore structure." 2nd Edition, Academic Press, New York.
- Dullien, F. A. L., and Dhawan, G. K. (1974). *Journal of Interface and Colloid Science*. **47**, 337.
- Ehrlich, R., Etris, E. L., Brumfield, D., Yuan, L. P., and Crabtree, S. J. (1991) "Petrography and Reservoir Physics III: Physical Models for Permeability and Formation Factor." *AAPG Bulletin*, **75**, 1579.
- Ferm, J. B., Ehrlich, R., and Crawford, G. A. (1993). "Petrographic Image Analysis and Petrophysics: Analysis of crystalline carbonates from the permian basin, West Texas." *Carbonates and Evaporites*, **8**, (1), 90.
- Gelhar, L.W. and Axness, C.L. (1983). "Three-dimensional stochastic analysis of macrodispersion in aquifers." *Water Resources Research*, **19**, 161.
- Ioannidis, M., and Chatzis. I. (1993). "A mixed percolation model of capillary hysteresis and entrapment in mercury porosimetry." *Journal of Interface and Colloid Science*, **161**, 278.
- Ioannidis, M. A., Kwiecien, M. J., and Chatzis, I. (1995). "Computer-Enhanced Core Analysis: First Annual Technical Report." Porous Media Research Group, University of Waterloo.

- Ioannidis, M. A., Kwiecien, M. J., and Chatzis, I. (1996). "Statistical Analysis of the Porous Microstructure as a Method for Estimating Reservoir Permeability", *J. of Petr. Sci. & Eng.* 16, 251-261
- Jewlal, D.M. (1996) "Estimating the air permeability of porous media using statistical image analysis", M.A.Sc. Thesis, U. of Waterloo
- Katz, A., and Thompson, A. (1986). "Quantitative prediction of permeability in porous rock." *Physical Review B*, 34, 8179.
- Koplik, J., Lin, C., and Vermette, M. (1984). "Conductivity and Permeability from Micro geometry." *Journal of Applied Physics*, 56 (11) 3127.
- Kwiecien, M. J. (1994). "On the Comprehensive Characterization of Porous Media via Computer Reconstruction and Stochastic Modeling." Ph. D. Thesis, University of Waterloo.
- Kwiecien, M. J., Macdonald, I. F., and Dullien, F. A. L. (1990) "Three Dimensional Reconstruction of Porous Media From Serial Section Data." *Journal of Microscopy*, 159, 343.
- Lymberopoulos, and Payatakes, A. C. (1992). "Derivation of Topological, Geometrical and Correlational Properties of Porous Media from Pore-Chart Analysis of Serial Section Data." *Journal of Interface and Colloid Science*. 150, (1), 61.
- McCreech, C. A., Ehrlich, R., and Crabtree, S. J. (1991) "Petrography and reservoir physics II: Relating thin section porosity to capillary pressure, the association between pore types and throat size." *AAPG Bulletin*, 75, 1563.
- Wardlaw, N. C., and Cassan, J. P. (1978). "Estimation of Recovery Efficiency by Visual Observation of Pore Systems in Reservoir Rocks." *Bulletin of Can. Petr. Geologists*, 26, (4), 572.
- Yuan, L. (1989) "Image analysis of pore size distribution and its application", in *Statistical Applications in the Earth Sciences*, ed Agterberg, F. P., and Bonham-Carter, G. F.; Geological Survey of Canada, Paper 89-9, 99.

Table 1: Core Analysis Data and Statistics of Image Analysis

Results of Core Analysis				Image Analysis Results					
Formation	Core Sample	Core ϕ	k (mD)	Pixel size (μm)	No. of Images	Avg. $\langle\phi_i\rangle$	Integral scale of ACF, $\langle I_i \rangle$ (μm)		Average specific surface area, S (μm^{-1})
							(1)	(2)	
Pekisko (dolomite)	58A	0.197	728	3.13	58	0.204	59.85	53.1	0.0241
	45A	0.153	25.9	1.54	69	0.149	23.55	22.58	0.0522
	45B	0.129	28.0	1.54	68	0.130	29.34	26.63	0.0380
	35B	0.101	3.51	1.54	61	0.109	41.54	39.0	0.0543
Montney (dolomitic siltstone)	9B	0.152	5.29	1.05	69	0.119	7.59	7.40	0.0719
	31B	0.129	1.78	1.05	75	0.125	7.63	7.34	0.0846
	30B	0.122	2.09	1.05	48	0.125	7.61	7.44	0.0824
	31A	0.102	0.47	1.05	71	0.109	6.35	6.18	0.0864
Gilwood (sandstone)	16	0.202	646.0	3.13	70	0.192	45.49	44.77	0.0284
	15A	0.173	114.0	1.54	66	0.168	36.62	32.00	0.0538
	7	0.134	412.0	3.13	58	0.129	42.41	39.90	0.0158
	4B	0.069	1.65	3.13	58	0.113	62.18	45.36	0.0194
Viking (sandstone)	4A	0.198	6.5	1.54	70	0.197	21.83	20.44	0.0732
	1	0.125	3.0	1.54	75	0.117	27.92	25.27	0.0288

Table 2. Parameter values for Equation (10) obtained by various methods.

Method used	Parameter values	A	B	C	Sum of Residuals Squared	Correlation coefficient R ²
model -(i): Employ Eq.(7) for fitting the average ACF to determine the average integral, <I _i >		8969	5.734	1.672	1.647 E5	0.98
model -(ii): < I >, using numerical integration of ACF's of all images in a sample		6323	5.608	1.774	1.69 E5	0.98
model -(iii): use all CECA images		0.517	1.5928	2.3174	3.203 E5	0.794
model -(iv): Employ images within the 95% confidence region		3.894	2.459	2.2501	1.632 E5	0.987

Table 3: Comparison of predictions by various models based on Eq.(10) and Eq.(1)

Core Sample	Core ϕ	FRF F	k (mD)	Avg. < ϕ >	Integral scale of ACF, <I _i > (μm)		Average specific surface area, S (μm^{-1})	Predicted Permeability k (mD)		
					(1)	(2)		Model-I	Model-II	Model-IV
58A	0.197	24.2	728	0.204	59.85	53.10	0.0241	923	976	595
45A	0.153	40.3	25.9	0.149	23.55	22.58	0.0522	32.0	36.8	40.1
45B	0.129	46.8	28.0	0.130	29.34	26.63	0.0380	21.2	22.9	41.6
35B	0.101	--	3.51	0.109	41.54	39.00	0.0543	13.8	16.8	63.6
9B	0.152	54.1	5.29	0.119	7.59	7.40	0.0719	1.33	1.44	1.87
31B	0.129	--	1.78	0.125	7.63	7.34	0.0846	1.78	1.87	2.08
30B	0.122	40.1	2.09	0.125	7.61	7.44	0.0824	1.77	1.92	2.14
31A	0.102	--	0.47	0.109	6.35	6.18	0.0864	0.60	0.64	1.01
16	0.202	--	646.0	0.192	45.49	44.77	0.0284	412	513	349
15A	0.173	45.7	114.0	0.168	36.62	32.00	0.0538	133	134	118
7	0.134	66.6	412.0	0.129	42.41	39.90	0.0158	37.5	45	101
4B	0.069	76.6	1.65	0.113	62.18	45.36	0.0194	33.3	26.9	98
4A	0.198	--	6.5	0.197	21.83	20.44	0.0732	140	148	63.7
1	0.125	--	3.0	0.117	27.92	25.27	0.0288	10.6	11.6	28.5

Note:(1) and (2) in table above refer to methods (i) and (ii) for parameter values in Table 2.

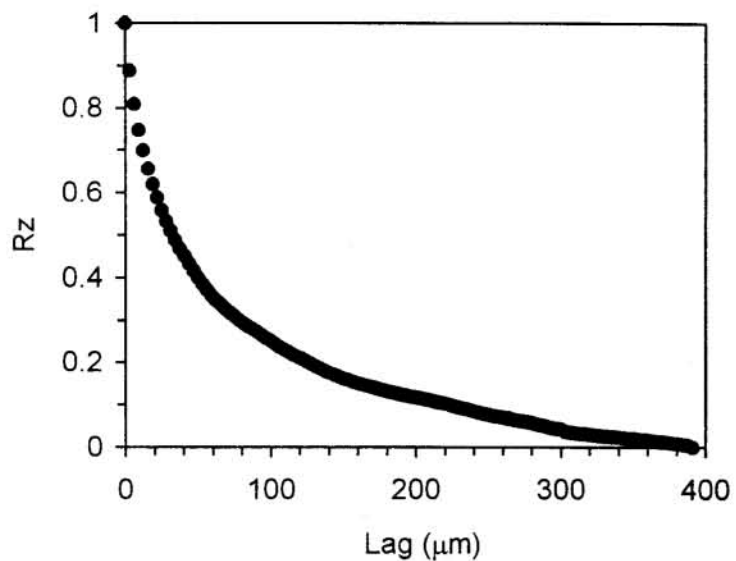


Figure 1. Typical autocorrelation function (ACF) for sample 58A (integral scale=72.4 μm).

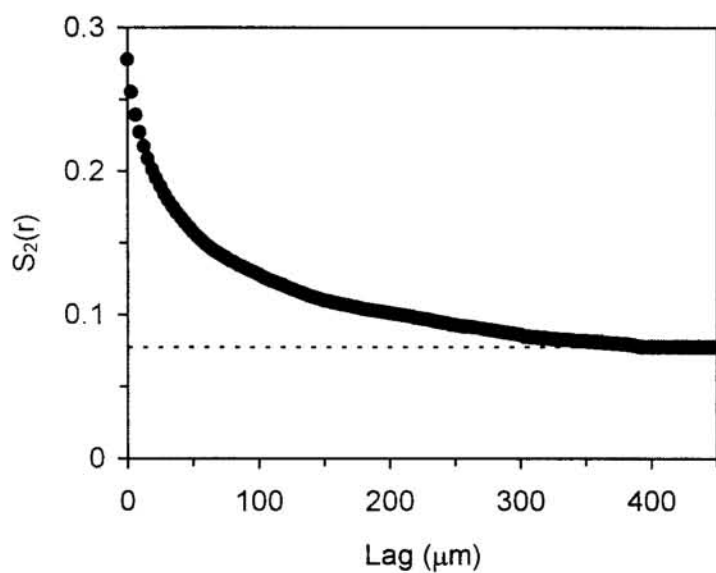


Figure 2. Typical 2-point correlation function for sample 58A.

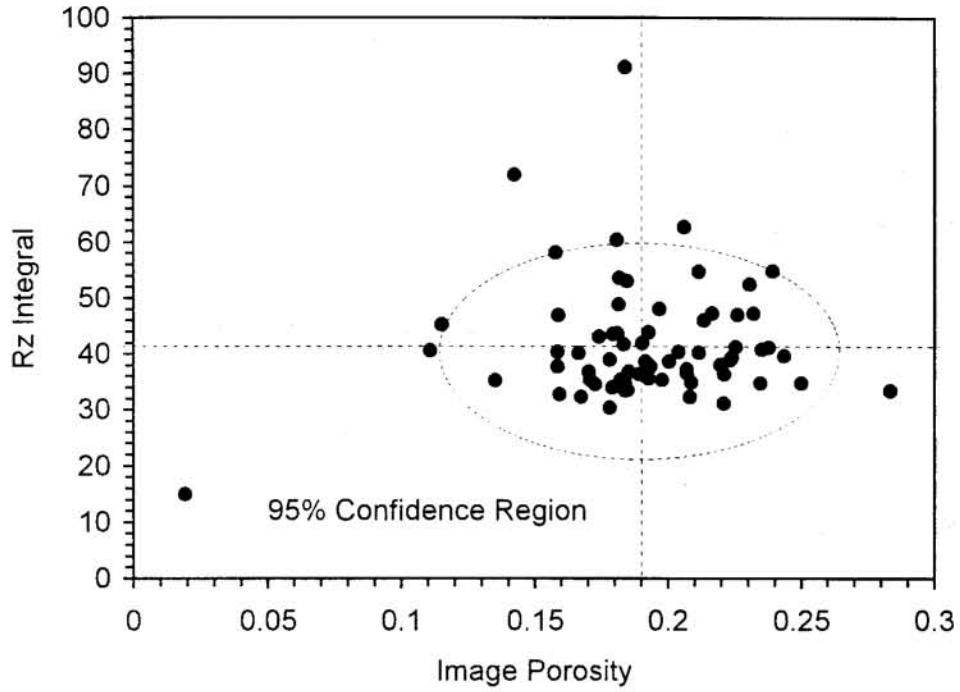


Figure 3. Integral scale of ACF vs. image porosity (sample 16).

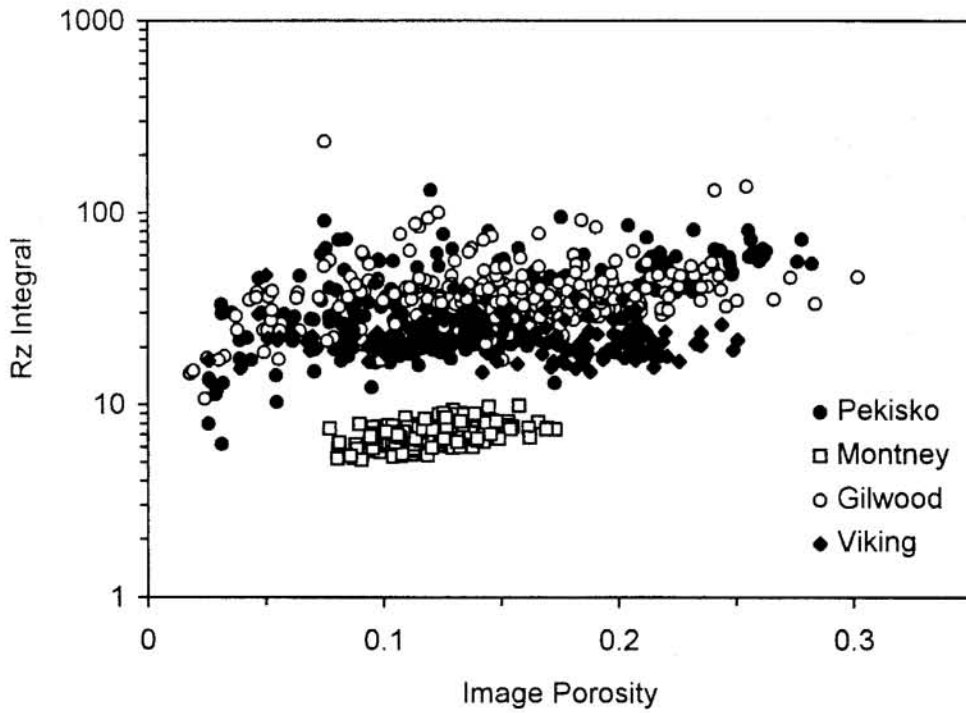
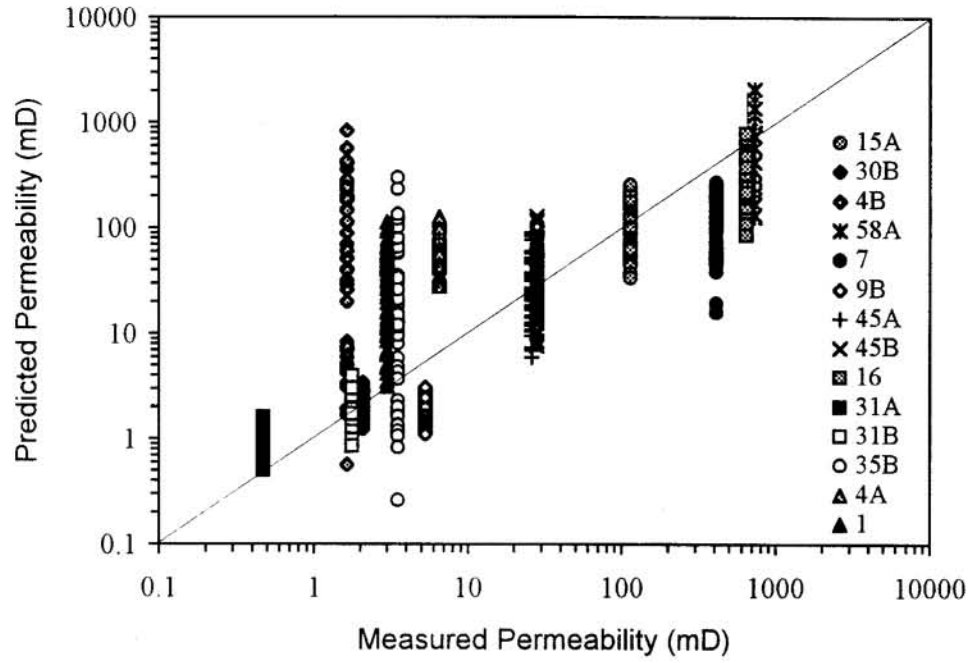
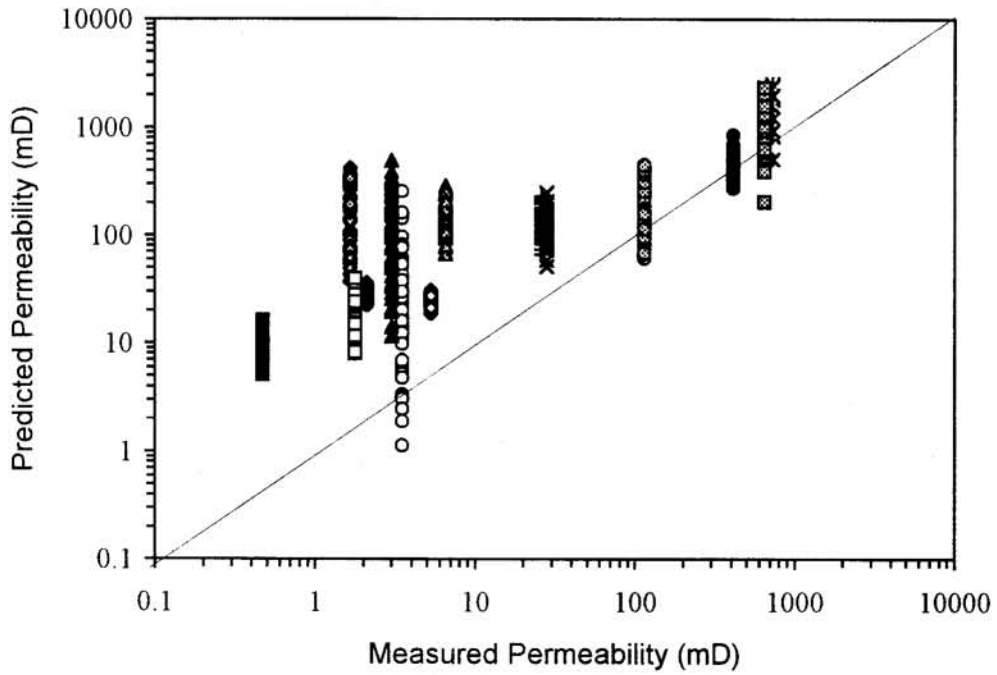


Figure 4. Integral scale of ACF vs. image porosity (all CECA data).



(a)



(b)

Figure 5. Permeability predictions from individual image data within the 95% confidence region: (a) Model IV; (b) Correlation of Berryman and Blair (1986).

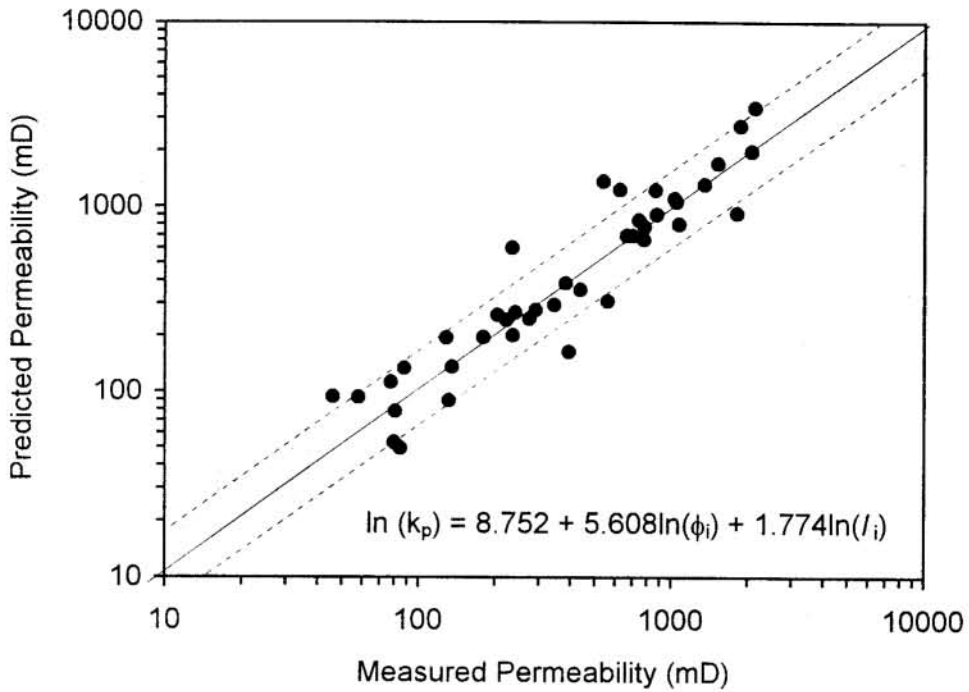


Figure 6. Prediction of the permeability of Coskun and Wardlaw's (1993) data set using model IV.

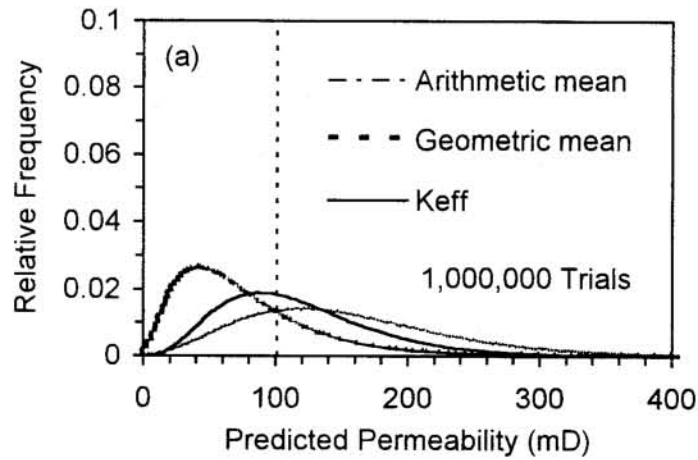


Figure 7. Monte Carlo permeability distributions of permeability estimates using a limited number of images: (a) sets of 10 images, (b) sets of 20 images, (c) sets of 40 images (sample 7).

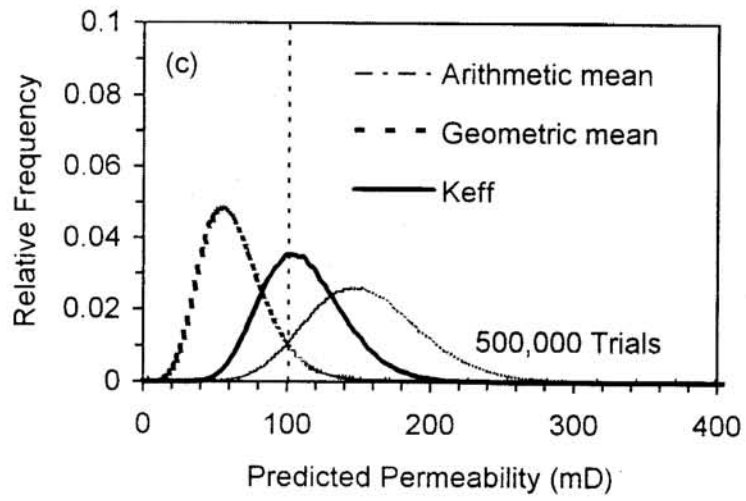
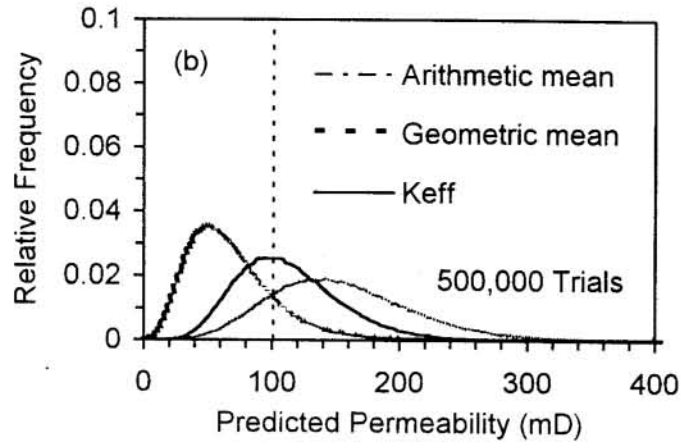


Figure 7. (continued)